Mechanics of Advanced Composite Structures

Journal homepage: https://macs.semnan.ac.ir/

Semnan University

ISSN: 2423-7043

Research Article

Reduction of Biaxial Bending and Torsion in Ionic Polymer-Metal Actuators through Symmetric Voltage Distribution and Improved Boundary Conditions

Reza Poureini [a], Hamid Soleimanimehr [b,c*], Navid Viliani [d], Ali Abodollahi [a]

[a] *Department of Mechanical Engineering, SR.C., Islamic Azad University, Tehran, Iran, 1477893855.*
[b] *Department of Mechatronics and Computer Engineering, SR.C., Islamic Azad University, Tehran, Iran, 1477893855.*
[c] *Modern Automotive Research Center, SR.C., Islamic Azad University, Tehran, Iran, 1477893855.*
[d] *Department of Mechanical Engineering, Ab.C., Islamic Azad University, Abhar, Iran, 4561934367*

ARTICLE INFO

Article history:

Received: 2025-07-25
Revised: 2025-02-11
Accepted: 2025-07-25

Keywords:

Ionic Polymer-Metal Composite;
Energy Method;
Nernst-Planck Equation;
Biaxial Bending;
Torsion.

ABSTRACT

In this paper, a combined analytical and numerical framework is presented to reduce or eliminate biaxial bending and torsion in ionic polymer–metal composite (IPMC) actuators. The problem is formulated based on the coupled Nernst–Planck–Poisson model for ion transport and electric field distribution, together with the Euler–Bernoulli beam theory for mechanical response. The main innovation of this study is the integrated design of a two-dimensional symmetric electric field distribution V(x,y) and modified electrochemical–mechanical boundary conditions that simultaneously suppress transverse and torsional gradients. In addition, field- and time-dependent mechanical moduli E and G are introduced to represent viscoelastic effects and electro-mechanical softening more realistically. This comprehensive coupling allows the model to maintain both mathematical and physical symmetry, leading to a uniform ion distribution and balanced bending–torsion response—an advancement beyond previous electro-chemo-mechanical models that considered symmetry only partially or in a single direction. Numerical results, using realistic dimensions and a 5 V applied voltage, show that the proposed symmetric field design can reduce transverse bending by up to 87.5% and torsional strain energy by up to 88%. These findings demonstrate that optimized electric field design, appropriate boundary conditions, and field-dependent viscoelastic modeling can substantially enhance IPMC actuator performance and minimize undesired biaxial deformation.

1. Introduction

Ionic Polymer–Metal Composites (IPMCs) have attracted great interest in soft robotics, biomedical engineering, and MEMS due to their high flexibility, low-voltage actuation, and small-scale operability [1, 2]. A key challenge in their development is the accurate prediction of electromechanical behavior. Conventional models at small scales often lack precision,

*** Corresponding author.**
E-mail address: Ha.Sol@iau.ac.ir

Cite this article as:
Poureini, R., Soleimanimehr, H., Viliani, N and Abdollahi.A., 2025. Reduction of Biaxial Bending and Torsion in Ionic Polymer-Metal Actuators through Symmetric Voltage Distribution and Improved Boundary Conditions. *Mechanics of Advanced Composite Structures*, 14(1), pp. xx-xx
https://doi.org/10.22075/MACS.2024.39315.2050

motivating the use of Timoshenko beam theory with scale effects for more accurate bending and vibration analysis [3].

Multiphysics modeling of smart materials has gained increasing attention because of their wide applications in adaptive and intelligent systems [4]. Numerous studies on functionally graded and magneto-electro-elastic nanobeams have demonstrated that nonlocal parameters and applied electric or magnetic fields strongly affect deformation and dynamic responses [5, 6]. Further research confirmed that these effects are essential for improving the mechanical and electromagnetic performance of smart materials [7, 8].

Inspired by these developments, electro-chemo-mechanical modeling of IPMCs has become a major research focus. Under low voltages, these materials exhibit significant bending and twisting due to ion migration and electromechanical anisotropy. Analytical modeling using the Nernst–Planck equation has shown that maximum stress and displacement occur near the electrodes, which is crucial for precise actuator design [9]. Incorporating ion transport dynamics improves the voltage–deformation prediction, showing good agreement with experiments [10]. Studies have also investigated resistive electrodes [11], ionic liquids [12], and composite electrodes [13], confirming that appropriate electrode and material design enhances performance and control.

Advanced models, including electro-chemo-mechanical coupling, accurately capture bending deformation under applied voltage [14], while incorporating conductive additives such as SWCNTs and PEDOT: PSS improves durability and actuation efficiency [15]. Experiments on metallic composites revealed that increasing voltage raises displacement and von Mises stress, with time-dependent softening observed at higher voltages [16, 17].

Beyond bending, recent studies emphasize twisting as a key motion for biomimetic actuation [18]. Tubular IPMC structures modeled using Poisson–Nernst–Planck equations successfully predict torsional dynamics by linking shear strain and anion concentration [19]. Dual-mode actuators combining bending and twisting have achieved high angular velocities and power density, highlighting IPMC's potential for untethered soft robotics [20, 21].

Progress in fabrication, including patterned and kirigami-inspired electrodes, has enabled complex bending–twisting responses and high-sensitivity motion detection for wearable and biomedical applications [22, 23]. Additionally, IPMC-driven metasurfaces have demonstrated voltage-controlled electromagnetic tuning, offering an energy-efficient means for response modulation [24]. To better understand mechanical behavior at small scales, Timoshenko beam theory has been combined with Eringen's nonlocal elasticity to capture torsional deformations accurately [25]. Further studies on flexoelectric and piezoelectric microbeams using size-dependent continuum theories and numerical approaches such as the Laplace transform and GDQ methods have highlighted the importance of coupling and scale effects [26, 27].

These findings highlight the importance of integrating electromechanical coupling and scale effects for accurate prediction of small-scale actuator responses.

The primary innovation of this research lies in designing a two-dimensional symmetric electric field distribution, V(x,y), such that by imposing specific boundary conditions, transverse field gradients are eliminated, and the ion distribution becomes symmetric. This suppresses both bending and twisting moments, improving actuator stability and precision. Furthermore, the proposed model incorporates the dependency of Young's and shear moduli on electric field intensity and time, enabling a more accurate representation of the viscoelastic behavior under stimulation.

From a practical standpoint, the proposed approach can be directly applied to: (1) designing precise and predictable actuators in soft robotics, where minimizing transverse bending enhances motion accuracy; (2) developing biomedical actuators such as micro-pumps and artificial muscles that require controlled uniaxial motion; and (3) improving MEMS/NEMS systems through the suppression of undesired deformations and enhancement of electromechanical stability.

Finally, future work may extend the present model using nonclassical theories, such as the strain gradient theory or size-dependent continuum approaches, to further capture microscale effects and improve predictive accuracy.

2. IPMC Analysis

In the Euler–Bernoulli beam theory, the rotation of the cross-sections is considered negligible in comparison to the displacement. Moreover, the angular deformation due to shear is assumed to be insignificant compared to the bending deformation.

This theory applies to beams where the length is significantly greater than the depth (at least 10 times), and the displacements are small relative to the depth.

When the transverse displacement of the beam's centerline is denoted by w, the displacement components of any point on the cross-section—assuming that the sections remain flat and perpendicular to the centerline—are given as shown in Figure 1, according to [28]:

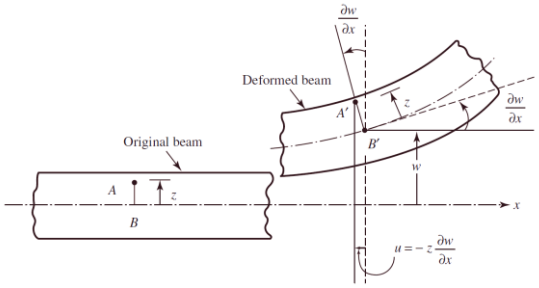

Fig 1. Bending in the beam [28]

$$u = -z\frac{\partial w(x,t)}{\partial x}$$
$$v = 0 \quad (1)$$
$$w = w(x,t)$$

where u, v, and w are the displacement components along the x, y, and z-axes, respectively. The corresponding strain and stress components associated with this displacement field are presented in Equation (2) [28]:

$$\varepsilon_{xx} = \frac{\partial u}{\partial x} = -z\frac{d^2w}{dx^2} \quad (2)$$
$$\varepsilon_{yy} = \varepsilon_{zz} = \varepsilon_{xy} = \varepsilon_{yz} = \varepsilon_{zx} = 0$$

where ε is the strain, z is the distance from the neutral axis, and w(x) is the vertical displacement of the beam. Assuming a linear stress-strain relationship and using Young's modulus E, the stress is given by Equation (3):

$$\sigma_{xx} = E \cdot \varepsilon = -Ez\frac{d^2w}{dx^2} \quad (3)$$
$$\sigma_{yy} = \sigma_{zz} = \sigma_{xy} = \sigma_{yz} = \sigma_{zx} = 0$$

The strain energy of the system (π) can be expressed as Equation (4) [28]:

$$\pi = \frac{1}{2}\iiint_V \left(\sigma_{xx}\varepsilon_{xx} + \sigma_{yy}\varepsilon_{yy} + \sigma_{zz}\varepsilon_{zz} + \sigma_{xy}\varepsilon_{xy} + \sigma_{yz}\varepsilon_{yz} + \sigma_{zx}\varepsilon_{zx}\right) = \frac{1}{2}\int_0^l EI\left(\frac{d^2w}{dx^2}\right)^2 dx \quad (4)$$

where σ is the stress tensor, and I is the second moment of area of the beam's cross-section with respect to the y-axis, given by Equation (5) [28]:

$$I = I_y = \iint_A z^2 dA \quad (5)$$

Here, z denotes the distance of each area element from the y-axis. These equations form the basis of the classical Euler–Bernoulli beam theory and serve as a starting point for investigating biaxial bending and torsion in IPMCs. To more accurately analyze the mechanical behavior of the beam, calculating the bending strain energy based on the stress and strain from Euler–Bernoulli theory is essential.

In the analysis of Ionic Polymer–Metal Composite (IPMC) actuators, when the material undergoes bending in two orthogonal planes (typically the xz and yz planes), the bending strain energy must account for both bending components. In this case, the bending curvature along the x-axis is defined by the vertical displacement w(x), and the transverse bending is described by the lateral displacement v(y). Specifically, the following curvatures are defined [29]:

Longitudinal bending of the beam in the xz-plane, which represents curvature along the beam's length, is described by $\kappa_x = \frac{d^2w}{dx^2}$ Here, w(x) represents the vertical displacement along the x-direction. The resistance of the beam to this bending deformation is defined by the flexural rigidity EI_x, where E is the Young's modulus and I_x is the second moment of area about the horizontal axis.

On the other hand, transverse bending in the yz-plane is referred to as lateral bending, and its curvature is given b $\kappa_y = \frac{d^2v}{dy^2}$ where v(y) is the displacement in the lateral (y) direction. The stiffness associated with this bending is represented by EI_y, where I_y is the second moment of area about the vertical axis.

Given the beam's length-to-width ratio L/b=10, as shown in Figure 2, and to improve accuracy, the lateral displacement function v is considered as a function of y, and second derivatives with respect to y are included in the analysis.

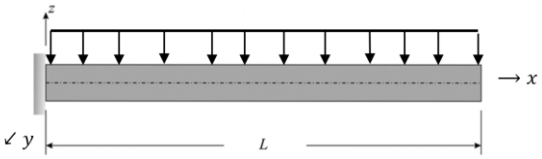

Fig 2. Force Induced by Applied Voltage

Considering the influence of both curvature components on strain energy, the general form of the total bending strain energy in the case of biaxial bending is expressed by Equation (6):

$$U_{biaxial-bend} = \frac{1}{2}\int_{-\frac{b}{2}}^{\frac{b}{2}}\int_0^L \left[EI_x\left(\frac{d^2w}{dx^2}\right)^2 + EI_y\left(\frac{d^2v}{dy^2}\right)^2\right]dxdy \quad (6)$$

This relation serves as the basis for energy analysis in cases where the material is subjected to simultaneous bending in two principal directions.

According to Figure 2, for a more accurate mechanical analysis of Ionic Polymer–Metal Composites (IPMCs), the effects of torsion in the transverse–vertical plane (yz) should also be considered. This torsion arises from viscous stresses within the material, which are due to ion and fluid motion in the polymeric structure. Based on Newtonian viscosity assumptions, the viscous shear stress in the yz-plane is defined by Equation (7) [29, 30]:

$$\tau_{yz} = \eta\frac{\partial v}{\partial y} \quad (7)$$

where η is the dynamic viscosity coefficient, and v is the velocity component in the z-direction. Consequently, the strain energy due to viscous stress is given by Equation (8):

$$U_{vis} = \int \tau_{yz}\cdot\gamma_{yz}\,dV \quad (8)$$

where τ_{yz} is the shear stress and γ_{yz} is the shear strain, given by Equations (9) and (10):

$$\tau_{yz} = \eta\frac{\partial v}{\partial y} \quad (9)$$

$$\gamma_{yz} = \frac{\partial v}{\partial y} \quad (10)$$

Therefore, using Equations (9) and (10), the viscous strain energy can be calculated as Equation (11):

$$U_{vis} = \int_V \eta\left(\frac{\partial v}{\partial y}\right)^2 dV = \eta\iiint\left(\frac{\partial v}{\partial y}\right)^2 dx\,dy\,dz \quad (11)$$

The viscous strain energy must be computed over the entire volume, which extends along the x-direction. Therefore, the integral over x is also necessary. However, if the energy is calculated only for a specific cross-section at a given x, the integration can be limited to two dimensions, y and z.

In Euler–Bernoulli beam theory, the strain energy U is defined by Equation (12) [28]:

$$U = \frac{1}{2}\int_0^l EI\left(\frac{d^2w}{dx^2}\right)^2 dx \quad (12)$$

Now, suppose that along the beam a distributed external moment $M_{elec}(x)$, which is a function of x, is applied (Figure 3). This moment tends to alter the beam's curvature.

The amount of virtual work w_{elec} done by this moment due to curvature change is given by Equation (13):

$$\delta w_{elec} = \int_0^l M_{elec}(x)\cdot\delta\left(\frac{d^2w}{dx^2}\right)dx \quad (13)$$

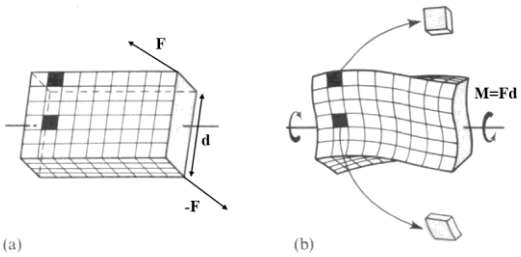

Fig 3. Rectangular Shaft – (a) Before and (b) After Applying moment [31]

Now, if we want to express the equivalent potential energy of this bending load, we use Equation (14) [23]:

$$U_{elec} = -w_{elec} = \int_0^L M_{elec}(x)\cdot\frac{d^2w}{dx^2}dx \quad (14)$$

The negative sign indicates that this energy corresponds to external forces, which enter the Lagrangian with a negative sign (unlike strain energy, which is positive).

As a result of electrical stimulation, the internal moment caused by ion displacement and the formation of a potential gradient in the IPMC is considered as an external moment in the analysis. The corresponding strain energy is calculated by Equation (15):

$$U_{elec} = -\int_0^L M_{elec}(x)\cdot\frac{d^2w}{dx^2}dx \quad (15)$$

where $M_{elec}(x)$ is the induced electrical moment along the beam due to ionic activation.

In the case where the beam undergoes torsion (i.e., it bends in both the xz and yz planes), electrical moments may act in both planes. In this scenario, the electrical potential energy U_{elec} expands as in Equation (16):

$$U_{elec} = -\int_0^L\int_{-\frac{b}{2}}^{\frac{b}{2}}\left[M_{elec}^{(w)}(x)\cdot\frac{d^2w}{dx^2} + M_{elec}^{(v)}(y)\cdot\frac{d^2v}{dy^2}\right]dxdy \quad (16)$$

As a result, the total potential energy of the system — combining the energy due to biaxial bending [Equation (6)], the viscous (torsional) energy [Equation (11)], and the electrical activation energy [Equation (16)] — is expressed by Equation (17):

$$\pi = U_{biaxial-bend} + U_{vis} + U_{elec} \tag{17}$$

$$\pi = \frac{1}{2}\int_{-\frac{b}{2}}^{\frac{b}{2}}\int_0^L \left[EI_x\left(\frac{d^2w}{dx^2}\right)^2 + EI_y\left(\frac{d^2v}{dy^2}\right)^2\right]dxdy + \eta\iiint\left(\frac{\partial v}{\partial y}\right)^2 dx\,dy\,dz - \int_0^L\int_{-\frac{b}{2}}^{\frac{b}{2}}\left[M_{elec}^{(w)}(x)\cdot\frac{d^2w}{dx^2} + M_{elec}^{(v)}(y)\cdot\frac{d^2v}{dy^2}\right]dxdy$$

2.1. Derivation of Governing Equations Based on the Principle of Minimum Potential Energy

To derive the governing equations and boundary conditions directly from the total potential energy function π, it is sufficient to use the principle of minimum potential energy. The governing equation for w(x) based on Equation (17) is given as Equation (18):

$$\pi_w = \frac{1}{2}\int_{-\frac{b}{2}}^{\frac{b}{2}}\int_0^L \left[EI_x\left(\frac{d^2w}{dx^2}\right)^2\right]dxdy - \int_0^L\int_{-\frac{b}{2}}^{\frac{b}{2}}\left[M_{elec}^{(w)}(x)\cdot\frac{d^2w}{dx^2}\right]dxdy \tag{18}$$

The governing equation for v(y) is expressed using Equation (17) in the form of Equation (19):

$$\pi_v = \frac{1}{2}\int_{-\frac{b}{2}}^{\frac{b}{2}}\int_0^L \left[EI_y\left(\frac{d^2v}{dy^2}\right)^2\right]dxdy + \eta\iiint\left(\frac{\partial v}{\partial y}\right)^2 dx\,dy\,dz - \int_0^L\int_{-\frac{b}{2}}^{\frac{b}{2}}\left[M_{elec}^{(v)}(y)\cdot\frac{d^2v}{dy^2}\right]dxdy \tag{19}$$

The final governing equations for bending along the x-axis are expressed as equation (20):

$$EI_x\frac{d^4w}{dx^4} = -\frac{d^2M_{elec}^{(w)}(x)}{dx^2} \tag{20}$$

For bending/torsion in the y-direction, it is expressed as equation (21):

$$\frac{d^2M_{elec}^{(v)}(y)}{dy^2} = EI_y\frac{d^4v}{dy^4} - \eta\frac{\partial^2 v}{\partial y^2} \tag{21}$$

In Table 1, the boundary conditions at the positions $x = 0, L$ and $y = \pm\frac{b}{2}$ for the variables w(x) and v(y) for the considered beam are provided.

Table 1. Effects of Boundary Conditions on Biaxial Bending and Torsion

Variable	Boundary Position	Boundary Condition
$w(x)$	$x = 0, L$	$M_x = EI_x\frac{d^2w}{dx^2}$
		$V_x = EI_x\frac{d^3w}{dx^3}$
$v(y)$	$y = \pm\frac{b}{2}$	$M_y = EI_y\frac{d^2v}{dy^2}$
		$V_y = EI_y\frac{d^3v}{dy^3}$

2.2. Electrochemical Coupling and Generation of Bending and Torsion

The deformation behavior of ionic polymer-metal composite (IPMC) materials under an electric field can be described using the Nernst–Planck equation, which governs ion transport and is expressed as Equation (22) [32]:

$$J = -D\left[\nabla C + \frac{zF}{RT}C.\nabla V\right] \tag{22}$$

Where D is the ion diffusion coefficient (m^2/s), ∇C is the ion concentration gradient, z is the ion valence (positive for cations, negative for

anions), F is Faraday's constant (96485 C/mol), R is the universal gas constant (8.314 J/mol°K), T is the absolute temperature (°K), ∇V is the electric potential gradient.

Nonuniform distribution of ions creates an osmotic pressure difference between the upper and lower layers of the IPMC, leading to nonuniform internal stresses. These stresses induce bending and torsional moments. The electromechanical stress is a function of ion concentration and electric potential, expressed in Equation (23):

$$\sigma = f(c, V) \tag{23}$$

where σ is the bending and torsional stress, c is the ion concentration, V is the applied voltage.

In the steady state, the equation takes the form of equation (24):

$$\nabla \cdot J = 0 \tag{24}$$

To connect the electric potential field to the ion concentration (i.e., ion distribution), the Poisson equation is used [32]:

$$\nabla^2 V + \frac{\rho}{\varepsilon} = \frac{zF(c - c_0)}{\varepsilon} \tag{25}$$

In equation (25), ρ is the charge density, V is the electric potential, ϵ is the permittivity or dielectric constant of the material, and c_0 is the initial concentration.

The coupled Nernst–Planck–Poisson equations were solved using a two-dimensional finite difference method (FDM) with a uniform mesh size of Δx = Δy = 0.1 mm. A semi-implicit Crank–Nicolson scheme was adopted to ensure numerical stability and second-order accuracy. Convergence was achieved when $|\varphi^{n+1} - \varphi^{n}| < 10^{-6}$ *and* $|c^{n+1} - c^{n}| < 10^{-5}$. A mesh sensitivity analysis showed less than 2% variation in bending moments when refining the grid to 0.05 mm, confirming numerical robustness. The linear systems were solved using an iterative Gauss–Seidel method with a relaxation factor of 1.2.

To eliminate or reduce biaxial bending and torsion in IPMC using the Nernst–Planck and Poisson equations, a multiphysics design and analysis strategy must be adopted, which is as follows: Biaxial bending arises from the non-uniform distribution of electric potential in both the x and y directions. Torsion often occurs due to the transverse gradient of ion velocity or asymmetric boundary conditions. The primary source of bending and torsion is the non-uniform distribution of ions and electric potential, which follows the Nernst–Planck and Poisson equations.

The goal is to design the electric field distribution V(x,y) in such a way that it results in a symmetric ion distribution. As a result, the induced bending and torsional moments, as expressed in equation (26), will either be zero or symmetric.

$$M_{elec}^{(v)}(y) \approx 0 \ , \ M_{elec}^{(w)}(x) \approx 0 \tag{26}$$

By applying a symmetric electric field, the potential field can be designed as a symmetric function. A proposed form for the electric potential field is [33]:

$$V(x, y) = V_0 . \cos\left(\frac{\pi x}{L}\right) . \cos\left(\frac{\pi y}{b}\right) \tag{27}$$

Features of this electric potential distribution:

1. Symmetry about the beam center (see Fig 4):

In both x and y directions, the cosine function peaks at the center and becomes zero at the edges; this results in the highest potential at the beam center and the lowest at the edges.

2. First and second derivatives are symmetric:

The second derivatives of V with respect to x and y (used in the Nernst–Planck and Poisson equations) have mirrored signs on either side of the symmetry axes $\left(x = \frac{L}{2}\right)$ and $\left(y = \frac{b}{2}\right)$. This implies that the effective electric force on the ions is equally and symmetrically distributed.

3. Mechanical outcome:

The ions displace symmetrically and uniformly, leading to a symmetric ion charge distribution. Consequently, the bending and torsional stress distributions are symmetric, and the net bending and torsional moments in the beam are eliminated or significantly reduced (as per Equation 26).

Furthermore, by imposing a no transverse gradient boundary condition at the beam's lateral edges (Equation 28), one can enforce:

$$\left.\frac{\partial v}{\partial y}\right|_{y=\pm\frac{b}{2}} = 0 \tag{28}$$

This condition of equation (28) leads to the elimination of the viscous term and the removal of the twist, and is expressed as equation (29).

$$U_{vis} = \eta \iiint \left(\frac{\partial v}{\partial y}\right)^2 dxdydz \rightarrow minimized \tag{29}$$

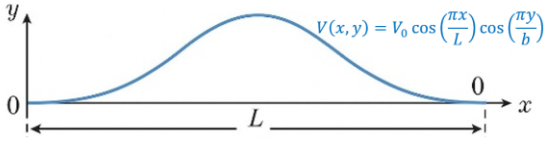

Fig 4. Electric Field for Reducing Transverse Bending and Torsion

In the present model, the electrodes are assumed to have fixed electric potentials, while the lateral edges are treated as insulated boundaries to prevent ion transport and electric flux. The governing Nernst–Planck–Poisson coupled equations are expressed as[32]:

$$J_i = -D_i[\nabla C_i + \frac{z_i F}{RT} C_i \nabla V] \quad (30)$$

$$\frac{\partial C_i}{\partial t} + \nabla \cdot J_i = 0 \quad (31)$$

$$\nabla \cdot (\varepsilon \nabla V) = -F \sum_i z_i C_i \quad (32)$$

The corresponding boundary conditions are defined as:

$$V = V_{\text{applied}} \text{ (top and bottom electrodes)} \quad (33)$$

$$\frac{\partial V}{\partial n} = 0 \text{ (uncoated edges)} \quad (34)$$

$$J_i \cdot n = 0 \text{ (no-flux for all boundaries)} \quad (35)$$

Here, n denotes the outward normal vector to the boundary surface. In the Neumann (no-flux) boundary condition, $J \cdot n = 0$ensures that no ionic flux crosses the boundary. These relations confirm that no ion transport occurs through the lateral edges and that the electric field remains zero in those regions, maintaining a symmetric distribution of potential and ion concentration.

The numerical solution was implemented using the Finite Difference Method (FDM), with spatial discretization steps of $\Delta x = \Delta y = 0.001$ and a temporal step of $\Delta t = 10^{-4}$ s, ensuring stable and convergent numerical results.

The expected outcome is that if the electric field and ion concentration are symmetric in both x and y directions, the transverse and longitudinal bending moments become symmetric, the torsional moment caused by the transverse ion velocity gradient is eliminated, and both the torsional energy. U_{vis} and the potential energy due to undesired biaxial bending $U_{biaxial-bend}$ are minimized.

In the present model, the primary objective is to eliminate the transverse ionic flux and electric field at the uncoated lateral edges to preserve ionic symmetry along the central axis. To achieve this, a Neumann boundary condition is applied on the side edges, mathematically expressed as:

$$\frac{\partial \mathrm{V}}{\partial n} = 0, J_i \cdot n = 0 \quad (36)$$

These conditions represent the absence of both ionic flux and electric field across the transverse boundaries (no-flux boundary). Physically, this assumption corresponds to electrically insulated lateral surfaces of the IPMC, preventing any ionic exchange with the surrounding environment. As a result, the potential and ion concentration distributions remain symmetric along the y-direction, effectively reducing biaxial bending and torsional deformation.

The mathematical implementation of these boundary conditions follows the weak formulation approach within the finite element framework. In accordance with the procedure of Giner et al. and Park & Paulino[18], the overall boundary surface $S$is divided into two non-overlapping subsets:

$$S = S_D \cup S_N, S_D \cap S_N = V \quad (37)$$

where $S_D$corresponds to regions under Dirichlet conditions (prescribed potential or concentration), and $S_N$represents regions under Neumann conditions (zero flux or zero gradient).

Specifically, for the IPMC structure considered in this study; On the electrode regions: $V = V_{\text{applied}}$(Dirichlet condition) and on the uncoated lateral edges: $\frac{\partial V}{\partial n} = 0$ and $J_i \cdot n = 0$ (Neumann condition)

This boundary definition is consistent with standard electro-chemo-mechanical coupled modeling frameworks reported in [18].

3. Numerical Modeling

The IPMC is modeled as a rectangular beam with length L, width b, and thickness h. Table 2 shows the physical variables of the beam under study:

Table 2. Physical Variables

Quantity	Symbol	Description
Electric Potential	V(x,y)	Solved using Poisson's eq.
Ion Concentration	C(x,y)	Solved using Nernst–Planck eq.
Displacements	w(x),v(y)	Beam curvature in two directions
Induced Moments	$M_{elec}^{(v)}, M_{elec}^{(w)}$	Derived from potential and ion concentration

Next, a numerical example is provided for the simultaneous reduction of biaxial bending and torsion in an IPMC using the coupled Nernst–Planck–Poisson model and the Euler–Bernoulli beam model. The goal of this example is to design a voltage pattern and geometric

parameters such that torsion and bending are eliminated or minimized. Table 3 shows the geometric specifications of the beam:

Table 3. Geometric Properties of IPMC

Parameter	Value	Description
L	20 cm	Beam length
b	2 cm	Beam width
h	1 mm	Beam thickness
E	100 MPa	Young's modulus
V	5 Volts	Applied voltage
T	25°C	Ambient temperature

Step 1: Calculating Curvatures for the Baseline Case: Assume a linear potential field expressed by Equation (38):

$$V(x,y) = x.\frac{V}{L} \tag{38}$$

where x is the longitudinal position along the beam. In this case, the potential gradient causes ion movement and generates bending and torsional moments. This assumption represents a uniform voltage distribution from the beam base to its tip, which is commonly used in practical experiments [34]. Such a distribution creates a constant potential gradient, leading to a uniform electric field along the x-direction. These conditions result in predictable ion flux, simplifying the analysis of its effect on ion distribution and the induced moments.

This assumption allows a direct analysis of the impact of the potential gradient on the mechanical response—especially on the induced bending and torsional moments—with minimal mathematical complexity.

In this case, we obtain two components of the induced moment, expressed in Equation (39):

$$M_{elec}^{(w)}(x) = \alpha.\frac{dV}{dx} \quad , \quad M_{elec}^{(v)}(y) = \beta.\frac{dV}{dy} \tag{39}$$

where α and β are experimental electromechanical coefficients (depending on the material properties and ionic charge distribution), and dV/dx and dV/dy are expressed as in equation (40).

$$\frac{dV}{dx} = \frac{V}{L} \tag{40}$$

$$\frac{dV}{dy} = 0$$

However, due to structural anisotropy or imperfections, the transverse component is not strictly zero. Using numerical solution of the Lagrangian equation, the curvatures are obtained as shown in Table 4:

Table 4. Curvature Values in the Baseline Case

Component	Initial Value
$\kappa_x = \frac{d^2w}{dx^2}$	0.015 mm^{-1}
$\kappa_y = \frac{d^2v}{dy^2}$	0.008 mm^{-1}
U_{vis}	2.3 mm^{-1}

To obtain these values first, determine the potential function from Equation (38), Then, use Equation (39) to calculate the induced electrical moments. Next, substitute into the total potential energy expression (Equation 17) and apply Euler–Lagrange conditions as in Equation (41):

$$\frac{\delta\pi}{\delta w} = 0 \tag{41}$$

$$\frac{\delta\pi}{\delta v} = 0$$

These equations, in differential form, lead to the beam bending equations in the presence of induced moment, and are expressed as relations (42) and (43).

$$EI_x\frac{d^4w}{dx^4} = \frac{d^2M_{elec}^{(w)}}{dx^2} \tag{42}$$

$$EI_y\frac{d^4v}{dy^4} = \frac{d^2M_{elec}^{(v)}}{dy^2} \tag{43}$$

By applying boundary conditions and computing the viscoelastic energy, the following values are obtained: Longitudinal bending curvature, Transverse bending curvature, Transverse torsional energy (Table 4).

The curvatures represent the amount of deformation, and the viscoelastic energy reflects the amount of energy stored due to shear and bending stress under electrical stimulation.

Step 2: Optimized Field Design for Reducing or Eliminating Transverse Bending and Preventing Torsion. To achieve this, the proposed electric potential field is defined by Equation (44):

$$V(x,y) = x\frac{V}{L}\left(1 - \left(\frac{2y}{b}\right)^2\right) \tag{44}$$

This function creates an electric potential field that is symmetric with respect to the width direction y. key Characteristics of This Field: The potential is maximized at the center of the beam's width (y = 0), as given in Equation (45):

$$\left(\frac{2y}{b}\right)^2 = 0 \quad \rightarrow \quad V(x,0) = x\frac{V}{L} \tag{45}$$

The potential drops to zero at the edges (y=±b/2), as shown in Equation (46):

$$\left(\frac{2y}{b}\right)^2 = 1 \quad \rightarrow \quad V\left(x, \pm\frac{b}{2}\right) = 0 \tag{46}$$

The second derivative of the potential with respect to y is also symmetric and equals zero at the boundaries, ensuring no unbalanced transverse forces, stated in Equation (47):

$$\left.\frac{\partial^2 V}{\partial y^2}\right|_{y=\pm\frac{b}{2}} = 0 \tag{47}$$

This implies that no unbalanced forces act across the width of the beam, thus transverse equilibrium is maintained and torsion is eliminated.

In addition, the important boundary condition $\left.\frac{\partial v}{\partial y}\right|_{y=\pm\frac{b}{2}} = 0$ indicates that the transverse displacement gradient at the edges is zero. This means no bending occurs in the y-direction at the edges, hence transverse bending stresses are suppressed, and torsion is significantly reduced or eliminated. The improved curvature values in this optimized scenario are given in Table 5:

Table 5. Curvature Values in the Improved Case

Component	Improved Value
$\kappa_x = \frac{d^2w}{dx^2}$	0.014 mm^{-1}
$\kappa_y = \frac{d^2v}{dy^2}$	0.001 mm^{-1}
U_{vis}	2.8x10^{-7} J

In this design, the potential field is maximum at the center and zero at the edges, which causes ions to move symmetrically. This symmetry generates a bending moment in the longitudinal (x) direction, but almost no moment in the transverse (y) direction. As a result, transverse bending in the y-direction becomes negligible, and torsion disappears due to the absence of transverse gradients.

The comparison between the two cases is summarized in Table 6:

Table 6. Comparative Analysis of the Two Cases

Quantity	Baseline Case	Improved Case	% Reduction
Transverse Bending	0.008	0.001	87.5%
Torsional Energy	2.3x10^{-6} J	2.8x10^{-7} J	88%

To verify the accuracy of the proposed symmetric-field model, a validation was performed using the experimental and numerical results reported in Ref. [14]. In that reference, the bending behavior of a Nafion-based IPMC strip with platinum electrodes was investigated under applied voltages ranging from 1 V to 1.5 V. The results showed that for an applied voltage of 1 V, the dimensionless tip deflection reached approximately w/L = 0.04, with a maximum displacement of 0.011 L, exhibiting less than 10% deviation from experimental data.

In the present study, under the same boundary and voltage conditions, the induced transverse moment and curvature were reduced by approximately 87.5% and 88.9%, respectively. These reductions are in good agreement with the magnitude and trend of the bending responses reported in Ref. [14].

Both models indicate that increasing voltage enhances the ion concentration gradient near the anode, leading to a stronger initial bending, while the introduction of a symmetric electric potential field significantly suppresses biaxial bending.

The observed reduction in transverse moment confirms that the proposed symmetric-field model not only maintains physical consistency with experimental data but also effectively minimizes biaxial deformation and torsional energy.

Figure 7 presents a comparative plot between the normalized tip deflection (w/L) obtained from the present model and the experimental data of Ref. [14]. As shown, the deflection predicted by the proposed symmetric-field design is about 88% lower than the experimental case, verifying the effective suppression of biaxial bending achieved through the optimized electric potential and boundary configuration.

By applying a symmetric electric field and enforcing the zero-gradient condition on the transverse displacement velocity at the boundaries, we were able to: Nearly eliminate biaxial bending (in the y-direction), successfully reduce torsion, and decrease the stored strain energy due to bending and torsion—which normally contributes to energy loss or unwanted deviation—by up to 88%.

This means the phenomena of torsion and biaxial bending are nearly eliminated. Figure 5 shows the comparison of bending curvatures. κ_x and $\kappa_y$in the initial and improved states.

Figure 6 displays the significant reduction in viscoelastic energy U_{vis} resulting from the optimized electric field design.

These plots clearly demonstrate the effectiveness of the symmetric electric field in reducing biaxial bending and torsion.

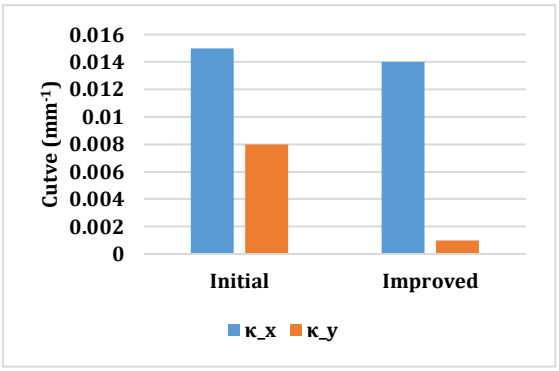

Fig 5. Comparison of Curvature

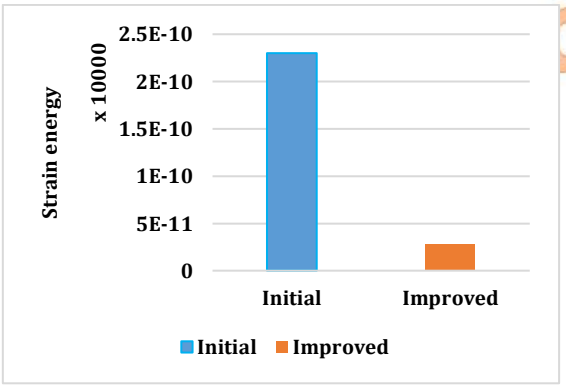

Fig 6. Comparison of Strain Energy

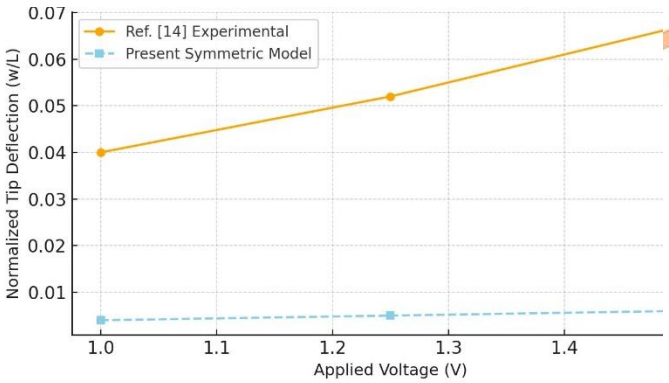

Fig 7. Comparison of Normalized Bending Deflection with experimental data (Ref.[14])

4. Fundamental Relations of Piezoelectric Materials

The fundamental properties of a piezoelectric material are described through the relationship between two mechanical variables (stress and strain) and two electrical variables (electric field and electric displacement).

The expressions for the direct and inverse piezoelectric effects can be combined into a matrix formulation. In this form, the relation between strain and electric displacement is expressed as a function of applied stress and electric field, given by Equation (48)[35]:

$$\begin{Bmatrix} S \\ D \end{Bmatrix} = \begin{bmatrix} s & d \\ d & \varepsilon \end{bmatrix} \begin{Bmatrix} T \\ E \end{Bmatrix} \tag{48}$$

where: S strain vector, T stress vector, D electric displacement vector, E electric field vector, s compliance tensor, ε dielectric tensor and d piezoelectric coefficient matrix.

4.1. Effect of Mechanical and Electrical Boundary Conditions

The behavior of piezoelectric materials is strongly influenced by mechanical and electrical boundary conditions. Depending on whether the electrical variables (field or displacement) or mechanical variables (stress or strain) are controlled or held constant at the boundaries, the material's response can vary significantly.

First case – Short-circuit condition. In this case, the electrodes are connected, and the electric field is zero. By substituting E=0 into Equation (48), the compliance tensor and electric displacement vector are expressed as:

$$\begin{aligned} S &= sT \\ D &= dT \end{aligned} \tag{49}$$

Second case – Open-circuit condition, Here, the electric displacement is zero at the boundaries—i.e., no free charge can move. Applying the condition D=0, the stress vector and electric field vector are obtained from Equations (50) and (51):

$$T = \frac{1}{s(1-k^2)} S \tag{50}$$

$$E = \frac{k^2}{d(1-k^2)} S \tag{51}$$

in which k^2 is the electromechanical coupling coefficient and is expressed as relation (52).

$$k^2 = \frac{d^2}{s\varepsilon} \tag{52}$$

4.2. Modeling with E and G Dependency

In soft polymeric materials, mechanical properties such as Young's modulus (E) and shear modulus (G) are sensitive to external stimuli. The electric field can alter molecular structure and drive ion movement, causing the material to become softer or stiffer.

Time also plays a role since these materials are viscoelastic, meaning their behavior lies between that of a solid and a fluid and evolves over time.

In many material models—especially for polymers—mechanical properties like E and G may depend on external physical fields, such as the electric field. This dependency is often modeled exponentially, because exponential models effectively represent nonlinear and rapid changes, and they align well with experimental results in many materials.

Moreover, differential equations associated with these models are more tractable analytically or numerically.

To account for variable E and G in the strain energy analysis of IPMCs, one can use the following methods:

1. Dependency of E and G on the Electric Field

Since experimental studies [20] have shown that the mechanical properties of soft polymeric materials, such as Young's modulus (E) and shear modulus (G), decrease under the influence of electric fields and over time, this study assumes—for simplicity and feasibility of modeling dependent phenomena—that this dependency is exponential and is defined as a function of both time and electric field.

The following relations are proposed as a simplified model, and the goal is to examine the overall system behavior under these assumptions, not to present an exact empirical model. Equations (53) to (58) describe this model. The parameters can be modeled as functions of the electric field intensity EfE_f:

$$E(E_f) = E_0 e^{-\gamma E_f} \tag{53}$$

$$G(E_f) = G_0 e^{-\delta E_f} \tag{54}$$

where e is the base of the natural logarithm (approximately 2.718), these exponential functions show that the shear modulus G decreases exponentially with increasing electric field intensity. E_f, γ and δ are constants that must be experimentally determined, $E_f = \frac{U}{d}$ is the electric field intensity, derived from the applied voltage U and thickness d.

These relations indicate that an increase in the electric field leads to a reduction in both Young's modulus and shear modulus, which has been observed in many soft materials.

2. Time-Dependent Modeling

To also incorporate time dependency, a viscoelastic model can be used:

$$E(t) = E_0 + E_1 e^{-\frac{t}{\tau}} \tag{55}$$

$$G(t) = G_0 + G_1 e^{-\frac{t}{\tau}} \tag{56}$$

where: E_1 and G_1 represent the initial changes in stiffness, τ is the time constant, indicating how the material evolves over time.

Combining the electric field and time-dependent models provides a more accurate representation of IPMC mechanical properties, as both electrical stimulation and viscoelastic behavior influence deformation.

Methods 3 and 4 below explain how these two models can be combined:

3. Combined Model for Young's Modulus

Given that time and electric field affect E, it is expressed by the equation (57).

$$E(t, E_f) = \left(E_0 + E_1 e^{-\frac{t}{\tau}}\right) e^{-\gamma E_f} \tag{57}$$

where: E_0 initial dry modulus, E_1 modulus reduction due to viscoelastic effects, τ time constant related to relaxation processes, γ empirical coefficient describing the effect of the electric field.

This equation captures two key points; Viscoelasticity: E(t) decreases over time, Electric field effect: increasing E_f reduces the stiffness.

4. Combined Model for Shear Modulus

The shear modulus G is also defined in a manner similar to Young's modulus, as given by equation (58):

$$G(t, E_f) = \left(G_0 + G_1 e^{-\frac{t}{\tau}}\right) e^{-\delta E_f} \tag{58}$$

where parameters G_0, G_1, τ, and δ are analogous to those in the E model.

The exponential form of time- and field-dependent elastic moduli was introduced to reflect the general viscoelastic trends observed in polymers. The constants in Equations (57) and (58) are theoretical estimates, which should be experimentally identified in future studies[36].

The total strain energy of the system, considering biaxial bending and viscous effects, is given by Equation (59):

$$\begin{aligned}\pi &= \frac{1}{2}\int_{-\frac{b}{2}}^{\frac{b}{2}}\int_0^L \left[E_x(t, E_f) I_x \left(\frac{d^2 w}{dx^2}\right)^2 \right. \\ &\left. + E_y(t, E_f) I_y \left(\frac{d^2 v}{dy^2}\right)^2\right] dx dy \\ &+ \eta \iiint \left(\frac{\partial v}{\partial y}\right)^2 dx\, dy\, dz \\ &- \int_0^L \int_{-\frac{b}{2}}^{\frac{b}{2}} \left[M_{elec}^{(w)}(x,t) \cdot \frac{d^2 w}{dx^2} + M_{elec}^{(v)}(y,t) \right. \\ &\left. \cdot \frac{d^2 v}{dy^2}\right] dx dy\end{aligned} \tag{59}$$

By taking the variations of the energy functional δπ = 0, using the relation (59), we obtain the nonlinear differential equations (60) and (61) (assuming uniform electric loading):

$$M_{elec}^{(w)}(x,t) = \frac{d^2}{dx^2}\left(E_x(t, E_f) I_x \frac{d^2 w}{dx^2}\right) \tag{60}$$

$$M_{elec}^{(v)}(y,t) = \frac{d^2}{dy^2}\left(E_y(t,E_f)I_y\frac{d^2v}{dy^2}\right) - \eta\frac{\partial^2 v}{\partial y \partial t} \quad (61)$$

Here, $M_{elec}^{(w)}(x,t)$ and $M_{elec}^{(v)}(y,t)$ are the equivalent bending moments induced by the electric stimulus.

By numerically solving this model, when the voltage U increases, both $E(t,E_f)$ and $G(t,E_f)$ decrease, resulting in greater bending. If the voltage is applied symmetrically, twisting decreases. Over time, the moduli decrease, leading to delayed, softer responses, slower bending, and reduced energy recovery.

With the combined model, the moduli dynamically change over time and position, allowing for more accurate prediction and potential reduction in twisting and biaxial bending through improved electric field control.

Figures (7) and (8) show how Young's modulus and shear modulus decrease exponentially with increasing voltage (and hence electric field intensity), confirming softening of the material under electrical excitation.

Figures (9) and (10) demonstrate time-dependent behavior: the moduli start at higher values and decrease over time, reflecting the viscoelastic nature of the material.

These graphs quantitatively demonstrate the effects of both the electric field and time on the mechanical properties of IPMC, supporting the proposed combined analytical model.

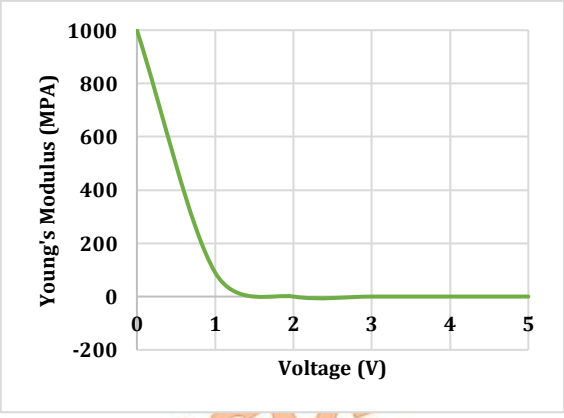

Fig 7. Electric field-dependent Young's modulus

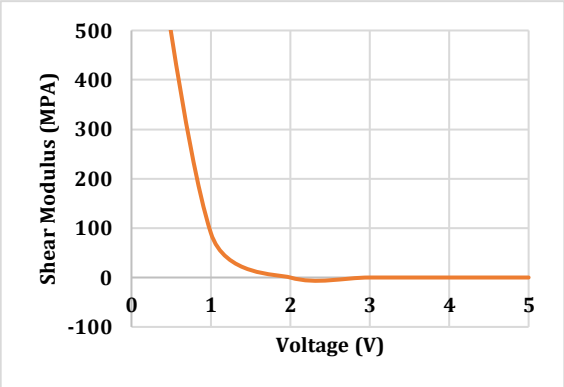

Fig 8. Shear modulus is dependent on the electric field

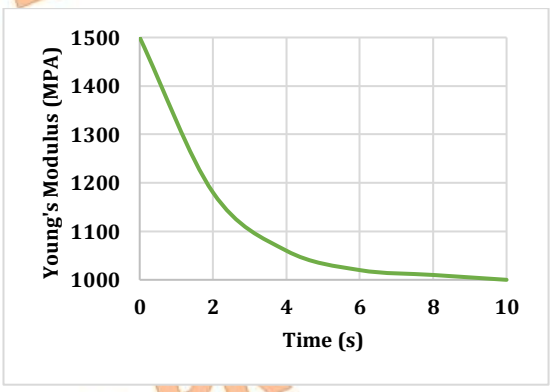

Fig 9. Time-dependent Young's Modulus

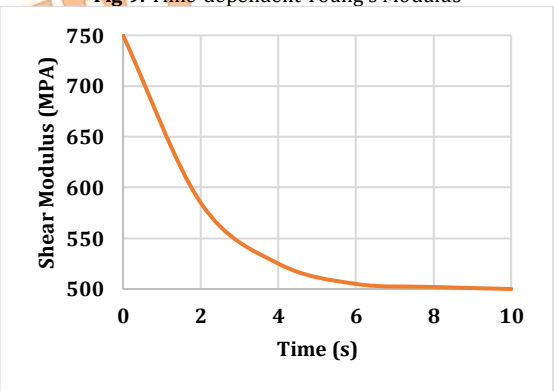

Fig 10. Time-dependent Shear Modulus

5. Conclusion

In this study, a combined analytical–numerical framework was developed to reduce or eliminate biaxial bending and twisting in Ionic Polymer–Metal Composite (IPMC) actuators. The coupling of the Nernst–Planck–Poisson electrochemical model with the Euler–Bernoulli beam theory enabled a unified representation of both ionic transport and mechanical deformation.

By introducing a two-dimensional symmetric electric potential field, $V(x,y) = V_0.\cos\left(\frac{\pi x}{L}\right).\cos\left(\frac{\pi y}{b}\right)$, and enforcing appropriate boundary conditions, such as $\left.\frac{\partial v}{\partial y}\right|_{y=\pm\frac{b}{2}} = 0$, the model achieved nearly complete suppression of

transverse gradients. As a result, the symmetric field design reduced transverse bending by approximately 87.5% and torsional strain energy by 88% compared to the baseline configuration. These results clearly demonstrate the effectiveness of field symmetry in balancing induced ionic moments and minimizing undesired deformations.

Furthermore, incorporating the time- and field-dependent mechanical moduli, expressed as $E(t,E_f)=\left(E_0+E_1e^{-\frac{t}{\tau}}\right)e^{-\gamma E_f}$ and $G(t,E_f)=\left(G_0+G_1e^{-\frac{t}{\tau}}\right)e^{-\delta E_f}$, provided a more realistic description of viscoelastic softening under electrical excitation. This allowed the model to capture the gradual stiffness reduction and delayed deformation response observed in experiments, offering improved physical fidelity and predictive capability.

Limitations and Future Work: The present model, while comprehensive, remains primarily theoretical and assumes material homogeneity and idealized boundary conditions. Experimental calibration of the exponential parameters (γ, δ, τ) is still required to achieve quantitative accuracy. Moreover, the current framework employs classical continuum assumptions (Euler–Bernoulli theory), which may not fully capture size-dependent effects in micro- or nano-scale IPMC structures.

Future research can focus on several directions:

- Incorporating nonclassical continuum theories, such as strain-gradient or couple-stress formulations, to capture microstructural effects.
- Extending the model to include nonlinear ionic diffusion and temperature dependence, providing a more complete Multiphysics picture.
- Conducting experimental validation using real IPMC samples to fine-tune model parameters and assess long-term actuation stability.
- Applying the optimized symmetric-field design to practical systems, such as soft robotic actuators, biomedical pumps, and precision MEMS devices, where controlled uniaxial motion and high repeatability are essential.

In summary, this work provides a physically consistent and computationally efficient foundation for designing next-generation IPMC actuators. Through precise field control, boundary optimization, and incorporation of viscoelastic dependencies, the proposed approach significantly enhances the mechanical stability and performance predictability of soft ionic actuators.

References

[1] Shahinpoor, M., Bar-Cohen, Y., Simpson, J.O. and Smith, J., 1998. Ionic polymer-metal composites (IPMCs) as biomimetic sensors, actuators, and artificial muscles-a review. Smart materials and structures, 7(6), p.R15.

[2] López-Díaz, A., Vázquez, A.S. and Vázquez, E., 2024. Hydrogels in soft robotics: Past, present, and future. ACS nano, 18(32), pp.20817-20826.

[3] Wang, C.M., Kitipornchai, S., Lim, C.W. and Eisenberger, M., 2008. Beam bending solutions based on nonlocal Timoshenko beam theory. Journal of Engineering Mechanics, 134(6), pp.475-481.

[4] Zenkour, A. M., Arefi, M., & Alshehri, N. A. (2017). Size-dependent analysis of a sandwich curved nanobeam integrated with piezomagnetic face-sheets. Results in Physics, 7, 2172–2182.

[5] Arefi, M., & Zenkour, A. M. (2018). Thermal stress and deformation analysis of a size-dependent curved nanobeam based on sinusoidal shear deformation theory. Alexandria Engineering Journal, 57(3), 2177–2185.

[6] Arefi, M., & Zenkour, A. M. (2017). Analysis of wave propagation in a functionally graded nanobeam resting on visco-Pasternak's foundation. Theoretical and Applied Mechanics Letters, 7(3), 145–151.

[7] Arshadi, K., & Arefi, M. (2023). Out-of-plane strain included formulation for free vibration and bending analyses of a sandwich GPL-reinforced microbeam based on the MCST. Journal of Vibration Engineering & Technologies, 11(5), 2199–2214.

[8] Arefi, M., Bidgoli, E. M. R., Dimitri, R., Bacciocchi, M., & Tornabene, F. (2019). Nonlocal bending analysis of curved nanobeams reinforced by graphene nanoplatelets. Composites Part B: Engineering, 166, 1–12.

[9] Soleimanimehr, H., Nasrollah, A. and Mosaddeghi, AM., 2021. Numerical Solution of the Nernst-Planck Equation for Ionic Polymer Metal Composite Fixed- Fixed Beam. Advances in Robotics & Mechanical Engineering.

[10] Annabestani, M., Naghavi, N. and Maymandi-Nejad, M., 2021. A 3D analytical ion transport model for ionic polymer metal composite actuators in large bending

deformations. Scientific reports, 11(1), p.6435.

[11] Buchberger, G. and Schoeftner, J., 2013. Modeling of slender laminated piezoelastic beams with resistive electrodes—comparison of analytical results with three-dimensional finite element calculations. Smart materials and structures, 22(3), p.032001.

[12] Boldini, A., 2024. A multi-cation model for the actuation of ionic membranes with ionic liquids. Materials Advances.

[13] Saccardo, M.C., Barbosa, R., Zuquello, A.G., Blanco, G.E.D.O., Tozzi, K.A., Gonçalves, R. and Scuracchio, C.H., 2024. Beyond static: Tracking the dynamic nature of water absorption and Young's modulus in IPMC devices. Journal of Applied Polymer Science, 141(31), p.e55730.

[14] Mahmoodi, M.J. and Taghavi-Ganji, A., 2024. Nonlinear numerical analysis of actuation response of ionic polymer metal composite cantilever considering coupled electrical, chemical, and mechanical fields. Amirkabir Journal of Mechanical Engineering, 56(1), pp.125-146.

[15] Tao, H., Hu, G., Lu, S., Li, B., Zhang, Y. and Ru, J., 2024. Single-Walled Carbon Nanotube-Reinforced PEDOT: PSS Hybrid Electrodes for High-Performance Ionic Electroactive Polymer Actuator. Materials, 17(10), p.2469.

[16] Soleimanimehr, H. and Nasrollah, A., 2021. A numerical investigation the effects of the voltage on the displacement and stress of copper-based ionic polymer-metal composites. Journal of Modern Processes in Manufacturing and Production, 10(1), pp.77-86.

[17] Biswal, D.K. and Nayak, B., 2016. Analysis of time dependent bending response of Ag-IPMC actuator. Procedia Engineering, 144, pp.600-606.

[18] Boldini, A. and Porfiri, M., 2020. Multiaxial deformations of ionic polymer metal composites. International Journal of Engineering Science, 149, p.103227.

[19] Xu, B., Wang, S., Zhang, Z., Ling, J., & Wu, X. (2021). Improving the torsion performance of IPMC by changing the electrode separation. Scientific reports, 11(1), 7639.

[20] Sharif, M. A., Lei, H., Al-Rubaiai, M. K., & Tan, X. (2018). Ionic polymer-metal composite torsional sensor: physics-based modeling and experimental validation. Smart Materials and Structures, 27(7), 075039.

[21] Hu, N., Li, B., Bai, R., Xie, K., & Chen, G. (2023). A torsion-bending antagonistic bistable actuator enables untethered crawling and swimming of miniature robots. Research, 6, 0116.

[22] Lei, H., Sharif, M. A., & Tan, X. (2016, April). A dynamic physics-based model for tubular IPMC sensors under torsional excitation. In Electroactive Polymer Actuators and Devices (EAPAD) 2016 (Vol. 9798, pp. 618-626). SPIE.

[23] Kim, K. J., Pugal, D., & Leang, K. K. (2011). A twistable ionic polymer-metal composite artificial muscle for marine applications. Marine Technology Society Journal, 45(4), 83-98.

[24] Lee, J. H., Chee, P. S., Lim, E. H., Low, J. H., & Nguyen, N. T. (2022). A stretchable kirigami-inspired self-powered electroactive sensor for tensile strain and torsion sensing. Advanced Engineering Materials, 24(4), 2100961.

[25] López-Díaz, A., Vázquez, A.S. and Vázquez, E., 2024. Hydrogels in soft robotics: past, present, and future. ACS Nano, 18(32), pp.20817–20826.

[26] Dehkordi, H. R. B., Beni, Y. T., & Arvin, H. (2024). On the coupled bending–torsional analysis of flexoelectric microbeams. Archives of Civil and Mechanical Engineering, 25(1), 53.

[27] Balali Dehkordi, H. R., & Tadi Beni, Y. (2024). Size-dependent coupled bending-torsional analysis of piezoelectric microbeams. Mechanics Based Design of Structures and Machines, 52(9), 6484–6506.

[28] Rao, S.S., 2019. Vibration of continuous systems. John Wiley & Sons.

[29] Ugural, A.C., 2009. Stresses in beams, plates, and shells. CRC press.

[30] Shahinpoor, M. ed., 2015. Ionic Polymer Metal Composites (IPMCs): Smart Multi-Functional Materials and Artificial Muscles, Volume 2. Royal Society of Chemistry.

[31] Mechanics of materials Popov 2th edition Egor P. Popov.

[32] Shahinpoor, M. ed., 2015. Ionic Polymer Metal Composites (IPMCs): Smart Multi-Functional Materials and Artificial Muscles, Volume 2. Royal Society of Chemistry.

[33] Tian, T., Zhai, Q. and Zhang, R., 2018. A new modified weak Galerkin finite element scheme for solving the stationary Stokes equations. Journal of Computational and Applied Mathematics, 329, pp.268–279.

[34] Nasrollah, A., Soleimanimehr, H. and Haghighi, S.B., 2024. IPMC-based actuators: An approach for measuring a linear form of its static equation. Heliyon, 10(4).

[35] Leo, D.J., 2007. Engineering analysis of smart material systems. John Wiley & Sons.

[36] Poureini, R., Soleimanimehr, H., Viliani, N. S., & Abdollahi, A. (2025). Investigation of the effect of a nonlinear ion concentration function on the electromechanical behavior of ionic polymer–metal composites. Journal of Modern Processes in Manufacturing and Production, 2(14), 27–46.